



Article

Design Hybrid Porous Organic/Inorganic Polymers Containing Polyhedral Oligomeric Silsesquioxane/Pyrene/Anthracene Moieties as a High-Performance Electrode for Supercapacitor

Mohsin Ejaz ¹ , Maha Mohammed Samy ^{1,2}, Yunsheng Ye ¹, Shiao-Wei Kuo ^{1,3,*} and Mohamed Gamal Mohamed ^{1,2,*}

¹ Department of Materials and Optoelectronic Science, College of Semiconductor and Advanced Technology Research, Center for Functional Polymers and Supramolecular Materials, National Sun Yat-Sen University, Kaohsiung 804, Taiwan

² Chemistry Department, Faculty of Science, Assiut University, Assiut 71515, Egypt

³ Department of Medicinal and Applied Chemistry, Kaohsiung Medical University, Kaohsiung 807, Taiwan

* Correspondence: kuosw@faculty.nsysu.edu.tw (S.-W.K.); mgamal.eldin34@gmail.com (M.G.M.)

Abstract: We synthesized two hybrid organic–inorganic porous polymers (HPP) through the Heck reaction of 9,10 dibromoanthracene (A-Br₂) or 1,3,6,8-tetrabromopyrene (P-Br₄)/A-Br₂ as co-monomers with octavinylsilsesquioxane (OVS), in order to afford OVS-A HPP and OVS-P-A HPP, respectively. The chemical structures of these two hybrid porous polymers were validated through FTIR and solid-state ¹³C and ²⁹Si NMR spectroscopy. The thermal stability and porosity of these materials were measured by TGA and N₂ adsorption/desorption analyses, demonstrating that OVS-A HPP has higher thermal stability (T_{d10}: 579 °C) and surface area (433 m² g⁻¹) than OVS-P-A HPP (T_{d10}: 377 °C and 98 m² g⁻¹) due to its higher cross-linking density. Furthermore, the electrochemical analysis showed that OVS-P-A HPP has a higher specific capacitance (177 F g⁻¹ at 0.5 A F g⁻¹) when compared to OVS-A HPP (120 F g⁻¹ at 0.5 A F g⁻¹). The electron-rich phenyl rings and Faradaic reaction between the π-conjugated network and anthracene moiety may be attributed to their excellent electrochemical performance of OVS-P-A HPP.

Keywords: octavinylsilsesquioxane; porous organic–inorganic polymers; heck reaction; thermal stability; energy storage



Citation: Ejaz, M.; Samy, M.M.; Ye, Y.; Kuo, S.-W.; Gamal Mohamed, M.

Design Hybrid Porous Organic/Inorganic Polymers Containing Polyhedral Oligomeric Silsesquioxane/Pyrene/Anthracene Moieties as a High-Performance Electrode for Supercapacitor. *Int. J. Mol. Sci.* **2023**, *24*, 2501. <https://doi.org/10.3390/ijms24032501>

Academic Editor: Jing Yu

Received: 25 December 2022

Revised: 17 January 2023

Accepted: 19 January 2023

Published: 28 January 2023



Copyright: © 2023 by the authors. Licensee MDPI, Basel, Switzerland. This article is an open access article distributed under the terms and conditions of the Creative Commons Attribution (CC BY) license (<https://creativecommons.org/licenses/by/4.0/>).

1. Introduction

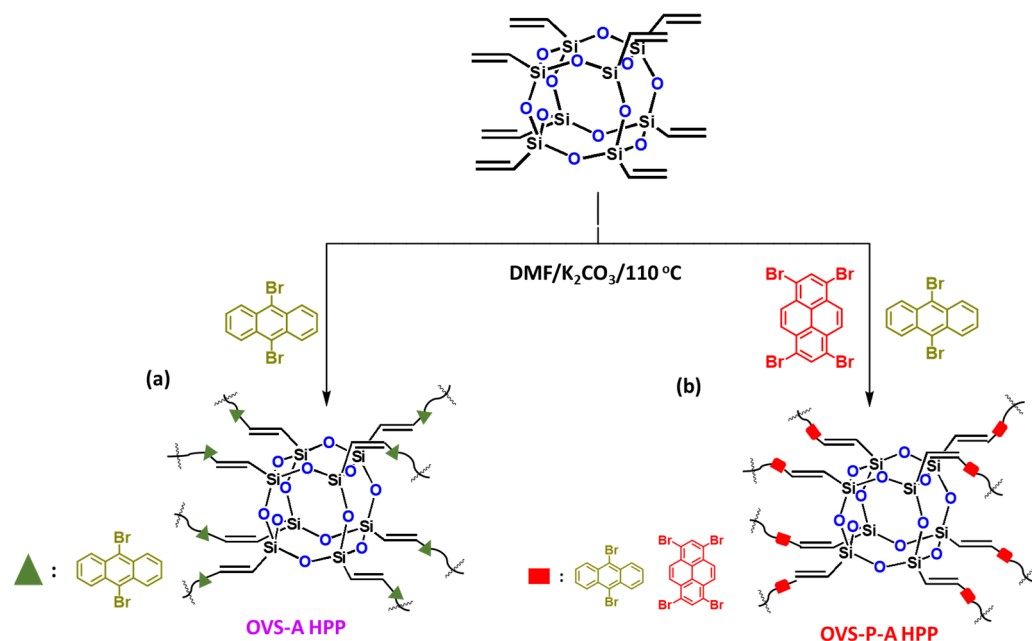
The disparity between the rising energy demand and the stagnant supply has resulted in a worldwide energy crisis [1–5]. The fast production and excessive use of fossil fuels have opened an urgent demand for providing solutions to environmental challenges. Therefore, there is a great need to innovate sustainable and effective energy storage methods [6–10]. Scientists have sought to address this problem by developing renewable energy storage methods. Supercapacitors (SCs) are one of the most practical approaches to addressing energy scarcity [11–13], and they have a high energy density, excellent durability, a quick charge/discharge mechanism, and significant stability [14–16]. In SCs, energy may be stored in two different ways; the first is the non-faradaic method, in which the ionic charges are gathered electrostatically at the electrolyte–electrode interface. In contrast, in the faradaic method, the activity occurs at the solid surface and involves a reversible redox reaction [17,18]. The electrode material is regarded as one of the main criteria influencing the effectiveness of SCs [19]. Thus, many inorganic, organic, and hybrid organic–inorganic materials have been used as electrode materials for SCs [20–24].

Designing new and stable electrode materials is still required to improve SC functionalities. Porous organic polymers (POPs) that have high surface areas, better thermal stability, porous characteristics, and exciting functions have attracted significant attention,

leading to their widespread usage in energy storage, optoelectronics, lithium-ion batteries, gas capture, and catalysis [25–29]. These outstanding functionalities of POPs make them attractive candidates as electrode materials for SCs [30–35]. POPs are further categorized into conjugated microporous polymers (CMPs), covalent organic polymers (COFs), and hyper-crosslinked polymers (HCPs) [36–40]. Polyhedral oligomeric silsesquioxane (POSS) is suitable for developing porous materials due to its rigid structure and high functionalization [41–45]. The existence of organic–inorganic hybrid components in POSS can provide both organic and inorganic characteristics to develop porous materials [45–50].

Octavinylsilsesquioxane (OVS) is the most efficient nanosized monomer (1–3 nm) among POSS derivatives due to its accessibility and cheap price [51,52]. OVS-based porous materials can be synthesized using various techniques, including Heck reactions, click reactions, Friedel–Crafts, and hydrosilylation [40–53]. OVS-based POPs materials have an impressive surface area, pore size, thermal stability, and electrochemical performance [54–58]. Furthermore, previous studies have shown that polycyclic aromatic hydrocarbons (PAH) could assist in enhancing energy storage performances [59]. Sandeep et al. presented different PAHs (pyrene, coronene, and triphenylene) as active cathode materials for organic batteries [60]. Kagatkar et al. synthesized pyrene-based chalcones electrode materials for supercapacitors that had a capacitance of 220 F g^{-1} [61]. We synthesized anthracene-based covalent organic frameworks that experienced a specific capacitance of 589 F g^{-1} [62]. Herein, we incorporated polycyclic aromatic hydrocarbons (pyrene and anthracene) into the backbone of OVS to enhance the super-capacitive performance.

In this study, we successfully synthesized two hybrids of a porous polymer-linked OVS unit through a Heck reaction of OVS with 9,10-dibromoanthracene (A-Br₂) and 1,3,6,8-tetrabromopyrene (P-Br₄)/A-Br₂ to obtain OVS-A HPP and OVS-P-A HPP, respectively (Scheme 1). Their chemical structures, thermal stability, porosity, morphology, and electrochemical performances are discussed below.



Scheme 1. Synthesis of (a) OVS-A HPP and (b) OVS-P-A HPP through Heck reaction.

2. Results and Discussion

2.1. Characterization, Thermal Stability, Porosity, and Morphology of OVS-A HPP and OVS-P-A HPP

The synthesis of two different hybrids of organic–inorganic HPP (OVS-A HPP and OVS-P-A HPP) is shown in Scheme 1. We synthesized A-Br₂ through the reaction of anthracene and Br₂ with chloroform at 50 °C for 4 h (Scheme S1). Then, we prepared

P-Br₄ by the reaction of pyrene with a neat Br₂ solution in nitrobenzene at 120 °C for 24 h (Scheme S2). Finally, we prepared OVS-A HPP and OVS-P-A HPP through the Heck reaction of A-Br₂ and P-Br₄/A-Br₂, respectively, with OVS, DMF, Pd(PPh₃)₄ and K₂CO₃ at 110 °C for 72 h (Scheme 1). All organic solvents showed a low solubility for these OVS-HPPs frameworks (Scheme 1), which is evident in the fact that the Heck reactions were effective, leading to the development of highly crosslinked OVS materials. The chemical structures of OVS-A HPP and OVS-P-A HPP were verified through FTIR and solid-state ¹³C and ²⁹Si spectroscopy, as shown in Figure 1. The absorption bands at 3113 cm⁻¹, 3067 cm⁻¹, 1610 cm⁻¹, and 1108 cm⁻¹ were found in the spectra of OVS, representing the bond stretching of C=CH, C=C, and Si-O-Si, respectively. The absorption band for A-Br₂, P-Br₄, OVS-A HPP, and OVS-P-A HPP were observed at 3073 cm⁻¹, 3031 cm⁻¹, 3079 cm⁻¹, and 3065 cm⁻¹, corresponding to C-H aromatics, respectively (Figure 1a,b). The development of cross-linked networks was also observed in both porous materials (OVS-A HPP, and OVS-P-A HPP), as the absorption spectra of the Si-O-Si unit were wider than that of OVS (Figure 1a,b). Furthermore, due to water absorption, both OVS-A HPP and OVS-P-A HPP featured OH groups in their FTIR spectra. According to the solid-state ¹³C NMR results of the OVS-A HPP and OVS-P-A HPP (Figure 1c), the carbon nuclei signals were found in the range 137–131 ppm and 148–127 ppm, respectively, representing aromatic carbons and C=C groups in both porous OVS-HPP-based materials. Additionally, solid-state ²⁹Si NMR analysis was used to verify the functional groups of OVS in the OVS-A HPP and OVS-P-A HPP structures. Figure 1d displays the signals that appeared near -11.2 ppm and -80.2 ppm, corresponding to Si-C=C and T₃ groups, respectively, for the OVS in the OVS-A HPP and OVS-P-A HPP.

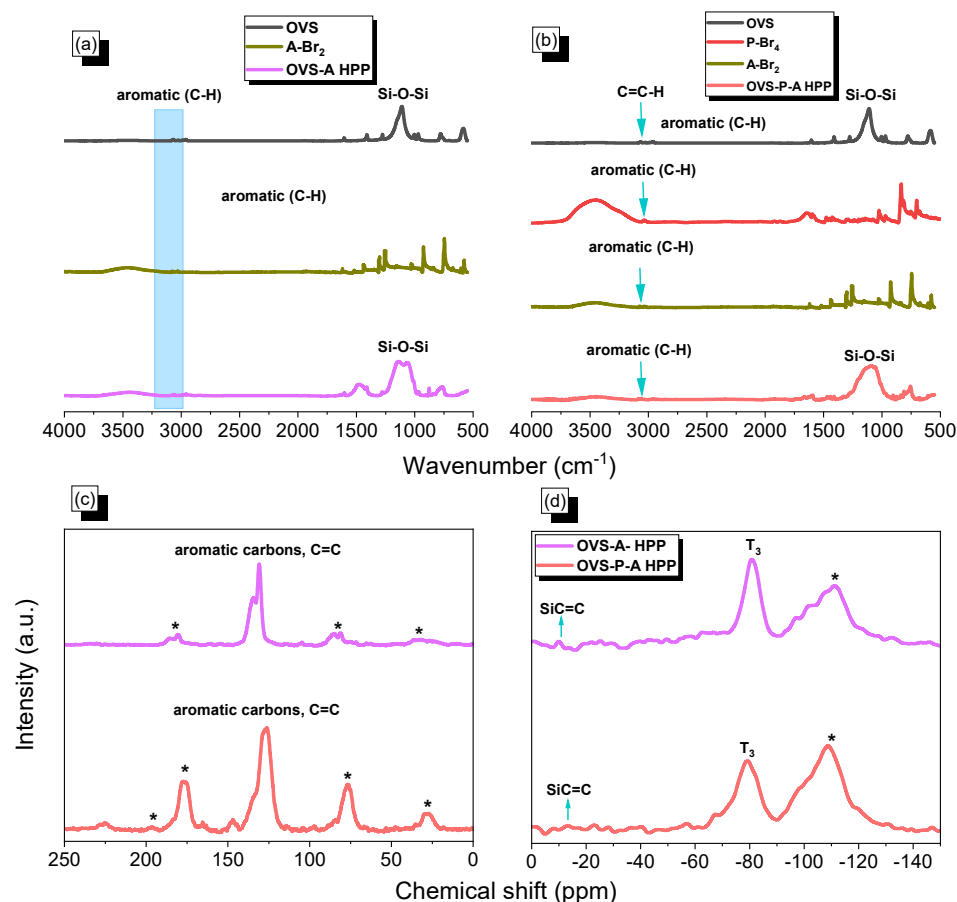


Figure 1. (a,b) FTIR of OVS, A-Br₂, P-Br₄, OVS-A HPP and OVS-P-A HPP, (c) ¹³C and (d) ²⁹Si NMR spectra of the OVS-A HPP and OVS-P-A HPP. * is the side band of solid-state nuclear magnetic resonance spectroscopy (NMR).

We performed X-ray photoelectron spectroscopy (XPS) to confirm the presence of Si, O, and C elements in OVS-A HPP and OVS-P-A HPP (Figure 2). We observed Si2p, Si2s, C1s, and O1s signals corresponding to 103 eV, 155 eV, 284 eV, and 532 eV for OVS-A HPP, respectively (Figure 2a), and 103 eV, 156 eV, 284 eV and 534 eV for OVS-P-A HPP, respectively (Figure 2b). XPS analysis confirmed the successful synthesis of OVS-A HPP and OVS-P-A HPP materials.

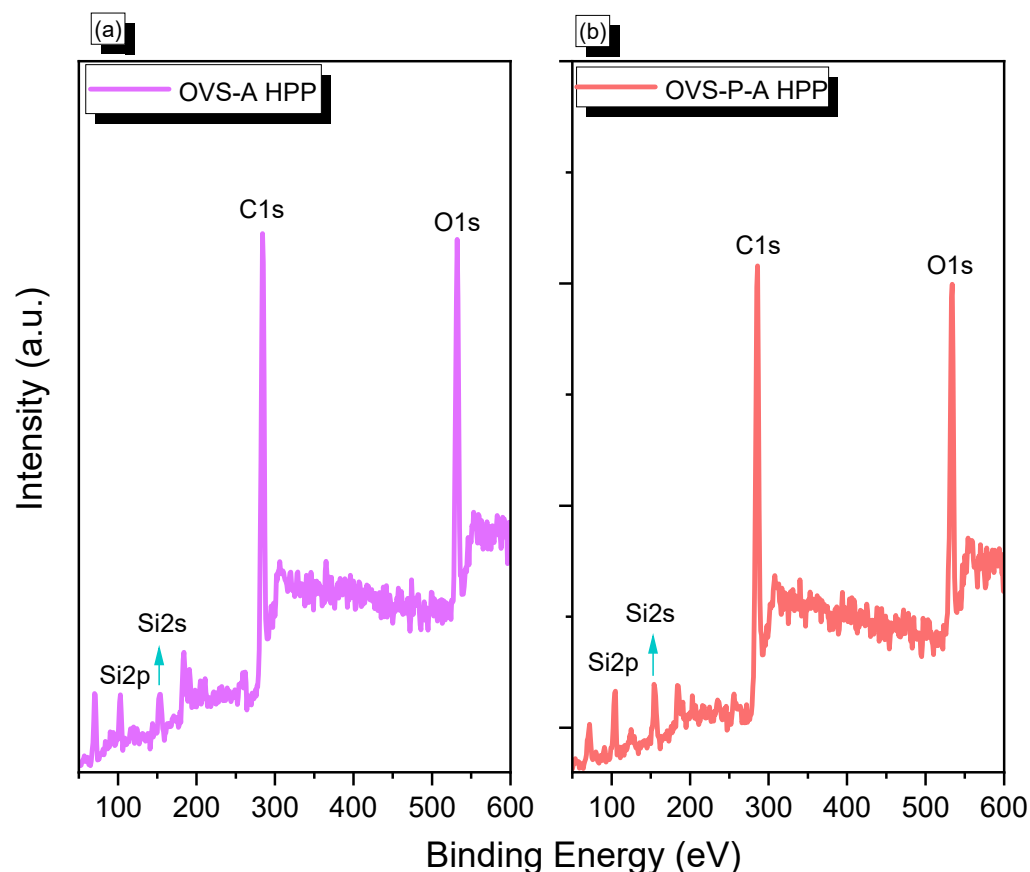


Figure 2. XPS analysis of (a) OVS-A HPP and (b) OVS-P-A HPP.

TGA analysis was used to measure the thermal stability and char yield of OVS-A HPP and OVS-P-A HPP (Figure 3). The thermal decomposition temperatures (T_{d5} , T_{d10}) and char yield for OVS were observed as 240 °C, 255 °C, and 4 wt%, respectively. The corresponding values for A-Br₂ were 219 °C, 234 °C, and 0 wt%, whereas those for P-Br₄ were 321 °C, 350 °C, and 0 wt%, respectively. We found that the developed hybrid porous material's thermal stability and char yield were greatly enhanced after the heck reaction, due to the cross-linking of OVS with A-Br₂ and P-Br₄/A-Br₂. The OVS-A HPP experienced a thermal stability of (T_{d5} , T_{d10}) 473 °C, 579 °C, and a char yield of 83 wt%; meanwhile, for OVS-P-A HPP, they were 317 °C, 377 °C, and 73 wt%, respectively. The thermal stability and char yield of OVS-A HPP was higher than that of OVS-P-A HPP due to its higher cross-linking density. The thermal properties of two hybrid porous materials are summarized in Table 1.

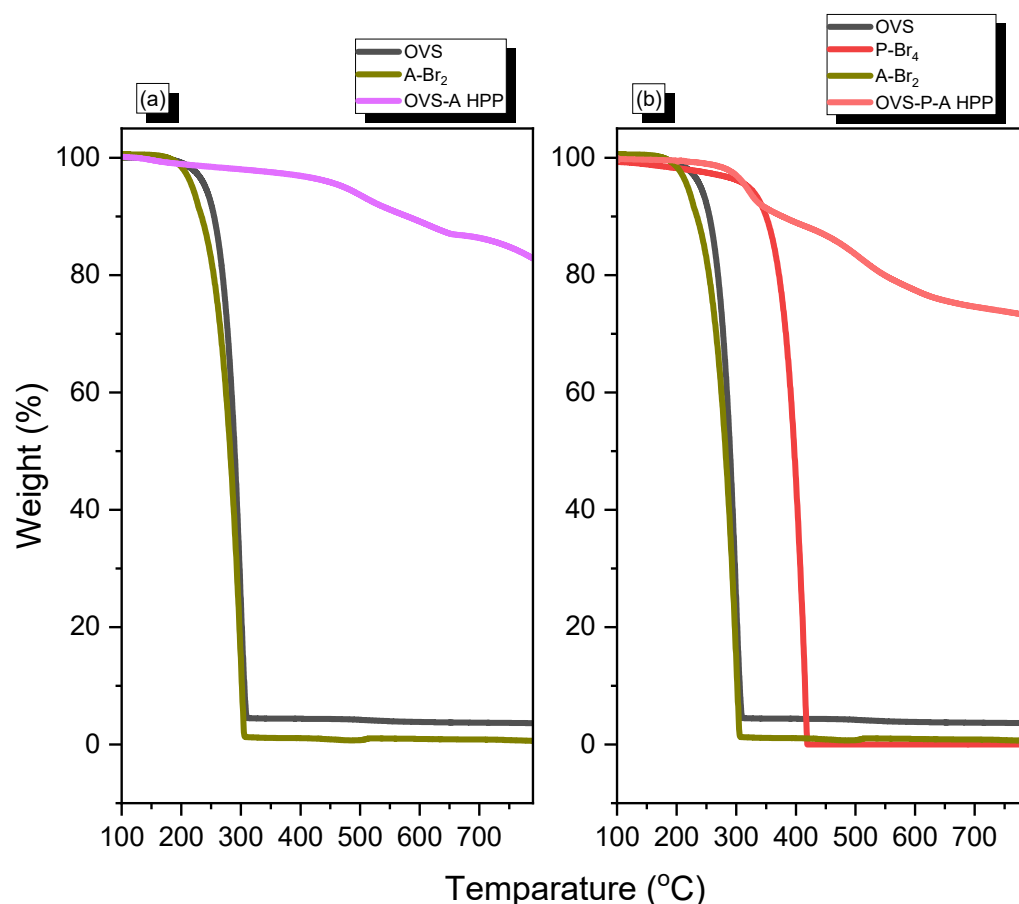


Figure 3. TGA analysis of (a) OVS, A-Br₂, OVS-A HPP and (b) OVS, P-Br₄, A-Br₂, OVS-P-A HPP.

Table 1. Thermal stability, porosity, and electrochemical performance of OVS-A HPP and OVS-P-A HPP.

Sample	T_{d10} (°C)	Char Yield (wt.%)	Surface Area (m ² /g)	Pore Volume (cm ³ /g)	Pore Size (nm)	Specific Capacitance at 0.5 A g ⁻¹ (F g ⁻¹)
OVS-A HPP	579	83	433	1.1	2	120
OVS-P-A HPP	376	73	98	0.3	2.5	177

The porosity properties of OVS-A HPP and OVS-P-A HPP were measured by N₂ adsorption/desorption (Figure 4a,b, and Table 1). The OVS-A HPP exhibited type II adsorption isotherm features, while the OVS-P-A HPP exhibited type II and IV according to the IUPAC classifications. The OVS-A HPP and OVS-P-A HPP exhibited rapid N₂ absorption uptake potentials in the low and high-pressure zones, indicating the presence of microporous and mesoporous in their structures. Furthermore, the surface area (S_{BET}) of OVS-A HPP (433 m² g⁻¹) was found to be higher than that of OVS-P-A HPP (98 m² g⁻¹). The OVS-A HPP and OVS-P-A HPP had mean pore diameters of ca. 2 nm and 2.5 nm, respectively, and their total pore volumes were 1.1 cm³ g⁻¹ and 0.3 cm³ g⁻¹, respectively (Figure 4c,d and Table 1).

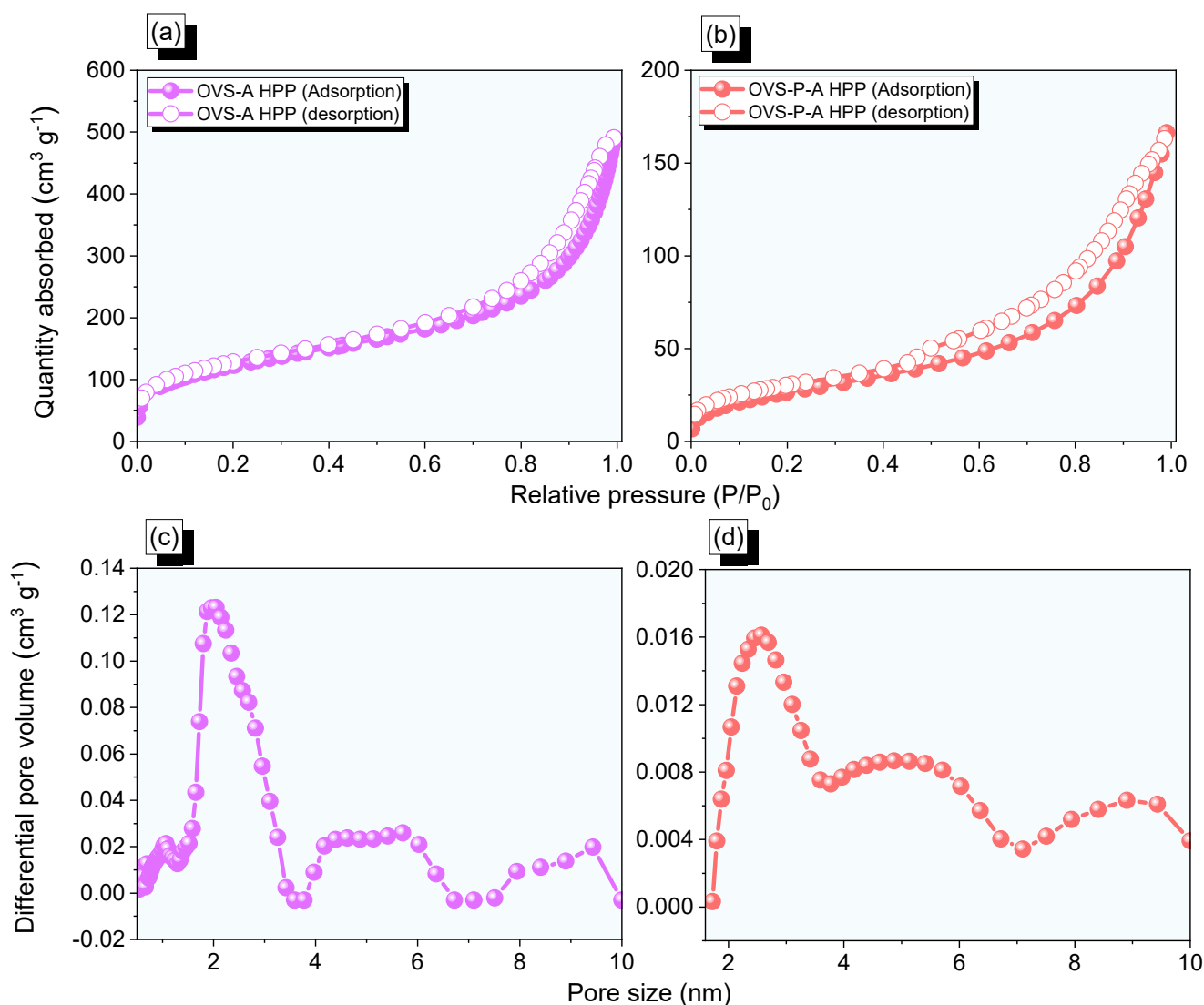


Figure 4. (a,b) N₂ isotherms profiles and (c,d) pore diameter size of the (a,c) OVS-A HPP and (b,d) OVS-P-A HPP.

The morphological and porous properties of OVS-A HPP and OVS-P-A HPP were investigated by SEM and TEM (Figure S3). The SEM images of OVS-A HPP showed clustered small spheres (Figure S3a), while for OVS-P-A HPP, we observed clustered irregularly shaped columnar and spheres (Figure S3b). The element mapping and energy dispersive X-ray (EDX) analyses of SEM images confirmed the existence of C, N, and O atoms (Figures 5 and 6). The corresponding weight percentages of C, N, and O atoms were found to be 48.3, 16.1, and 36% for OVS-A HPP, and 33.2, 13.3, and 54% for OVS-P-A HPP. Furthermore, the morphology of hybrid porous materials was further confirmed by the TEM images (Figure S3c,d). These images show small pores, confirming porous structure, and dark and bright patches representing amorphous characteristics in OVS-A HPP and OVS-P-A HPP.

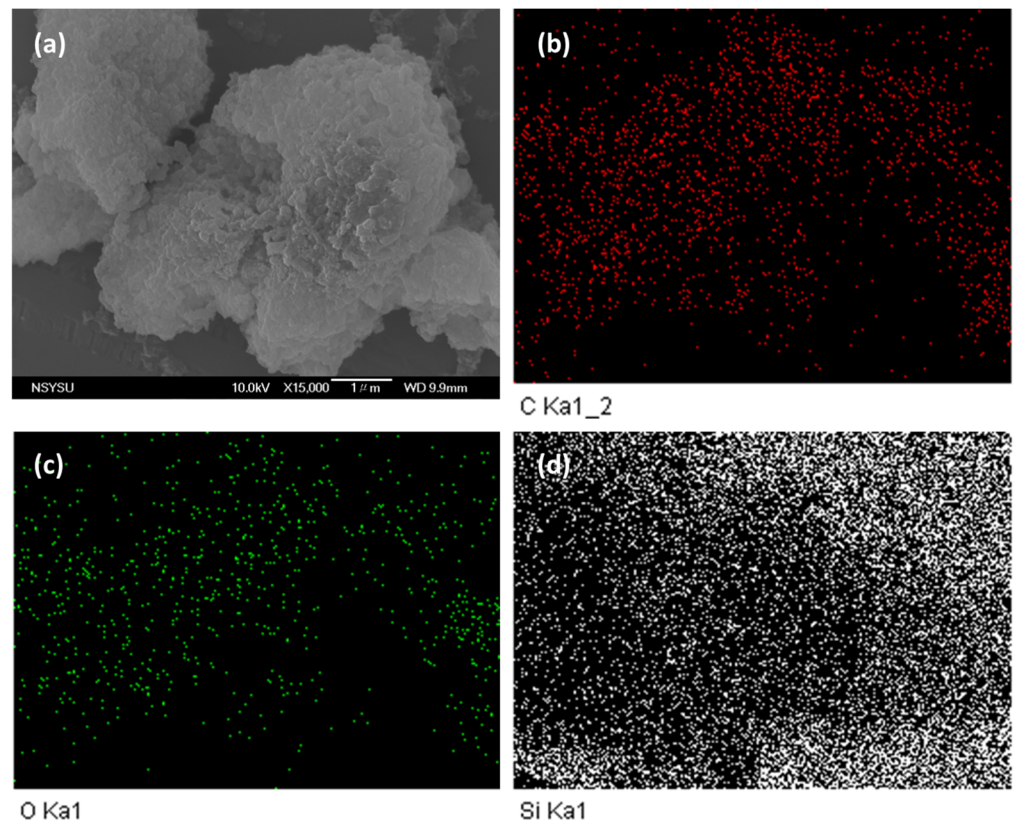


Figure 5. SEM images and their corresponding element mapping for (a–d) OVS-A HPP.

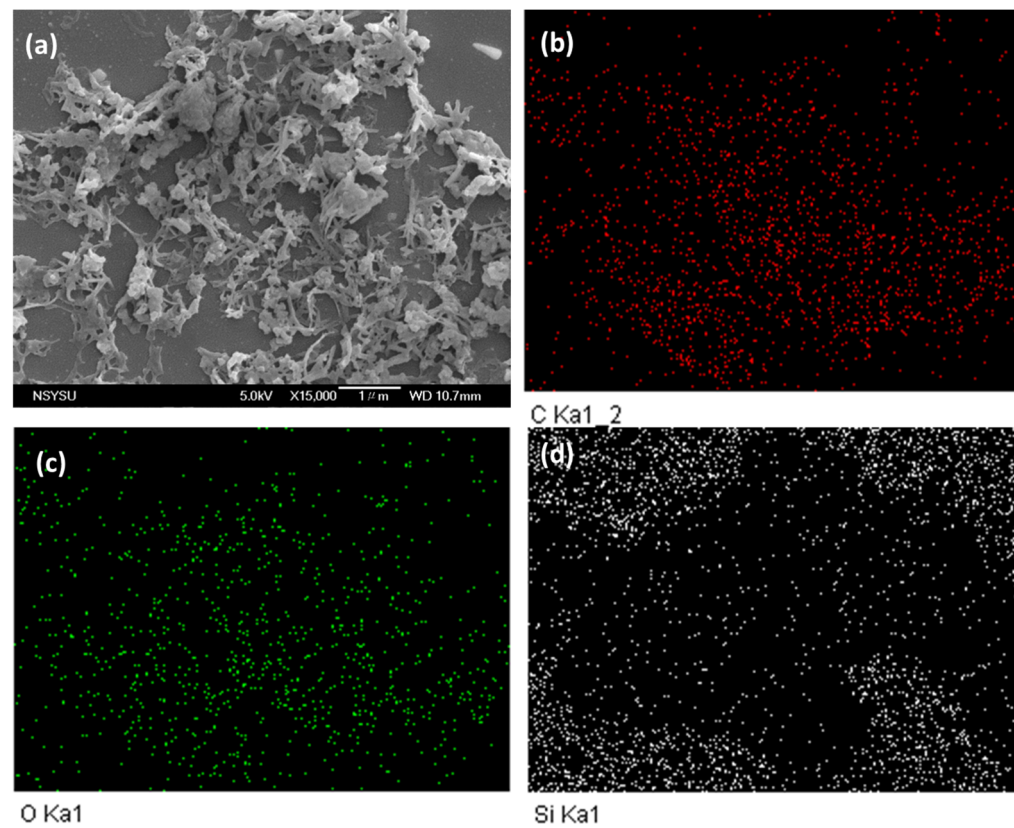


Figure 6. SEM images and their corresponding element mapping for (a–d) OVS-P-A HPP.

2.2. Electrochemical Properties of OVS-A HPP and OVS-P-A HPP

The electrochemical properties were investigated in a three-electrode cell (system), using the techniques for cyclic voltammetry (CV) and galvanostatic charge-discharge (GCD) in 1 M of KOH aqueous solution (Figure 7a–d). The CV profiles of OVS-A HPP and OVS-P-A HPP were measured at different scan rates (200 to 5 mV s^{-1}) and potential windows (-1 to 0 V) (Figure 7a,b). Both the samples experienced rectangular CV curves, with humps suggesting that this capacitive behavior occurred mostly from electric double-layer capacitance (EDLC) and pseudocapacitance [63]. Increasing the scan rate led to a higher specific current without changing the morphologies of the CV profiles, validating the stabilities and the efficient electron mobility [64]. The GCD curves of OVS-A HPP and OVS-P-A HPP were measured at different specific currents (0.5 to 20 A g^{-1}) (Figure 7c,d). The cathodic peaks can be seen for both electrode materials in CV plots, due to the presence of heteroatoms (O and Si) in the OVS unit and electron-rich phenyl groups in the anthracene and pyrene [53,55]. The GCD curve of OVS-A HPP showed an approximately rectangular curve with a small bend, demonstrating the combined effects of pseudocapacitance and EDLC [65]. The GCD curves of OVS-P-A HPP demonstrated the traditional characteristics of a pseudocapacitance with great symmetry, suggesting a strong electrochemical performance [66]. The discharge time of OVS-P-A HPP was higher and more prominent than OVS-A HPP (Figure 7c,d), showing its comparatively high capacitance.

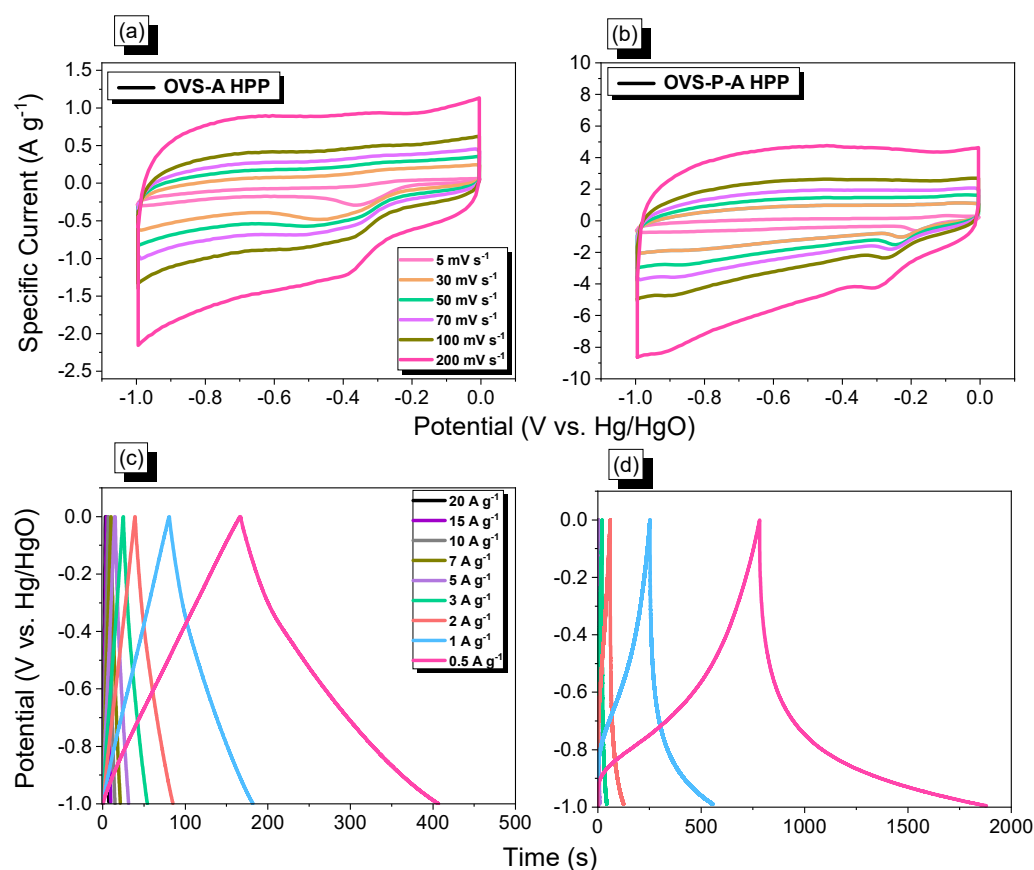


Figure 7. (a,b) CV and (c,d) G curves, of (a,c) OVS-A HPP and (b,d) OVS-P-A HPP.

The specific capacitances of OVS-A HPP and OVS-P-A HPP, calculated from GCD curves, were 120 F g^{-1} (calculated by using Equation (S1)) and 177 F g^{-1} (calculated by using Equation (S2)), respectively, at 0.5 A g^{-1} (Figure 8a). The difference in the specific capacitance between the OVS-A HPP and OVS-P-A HPP was very pronounced when the specific current was increased to 20 A g^{-1} , experiencing the values of 2 F g^{-1} and 2.5 F g^{-1} , respectively. As a result, the overall CV and GCD analysis showed that

OVS-P-A HPP showed higher electrochemical properties than OVS-A HPP. The chemical structure of OVS-P-A HPP contains pyrene groups with more electron-rich phenyl rings, allowing the electrolytes to reach the electrode surface more quickly than in the OVS-A HPP; this was responsible for its comparatively remarkable performance [67]. The Faradaic reaction between anthracene and the π -conjugated framework may also be responsible for OVS-P-A HPP's excellent performance. When the specific current was increased from 0.5 to 20 A g^{-1} , the specific capacitance of OVS-A HPP and OVS-P-A HPP declined, most likely because there was not enough time for ion mobility at such high specific currents [68]. The specific capacitance retention of OVS-A HPP and OVS-P-A HPP was also measured at 2000 cycles from GCD analysis (Figure 8b). The OVS-A HPP and OVS-P-A HPP exhibited excellent stability, with a specific capacitance retention of 85% and 98%, respectively. Additionally, the electrochemical performance of OVS-A HPP and OVS-P-A HPP was exceptional when compared to previously reported porous polymers and composite materials (Table S1) [53,69–75].

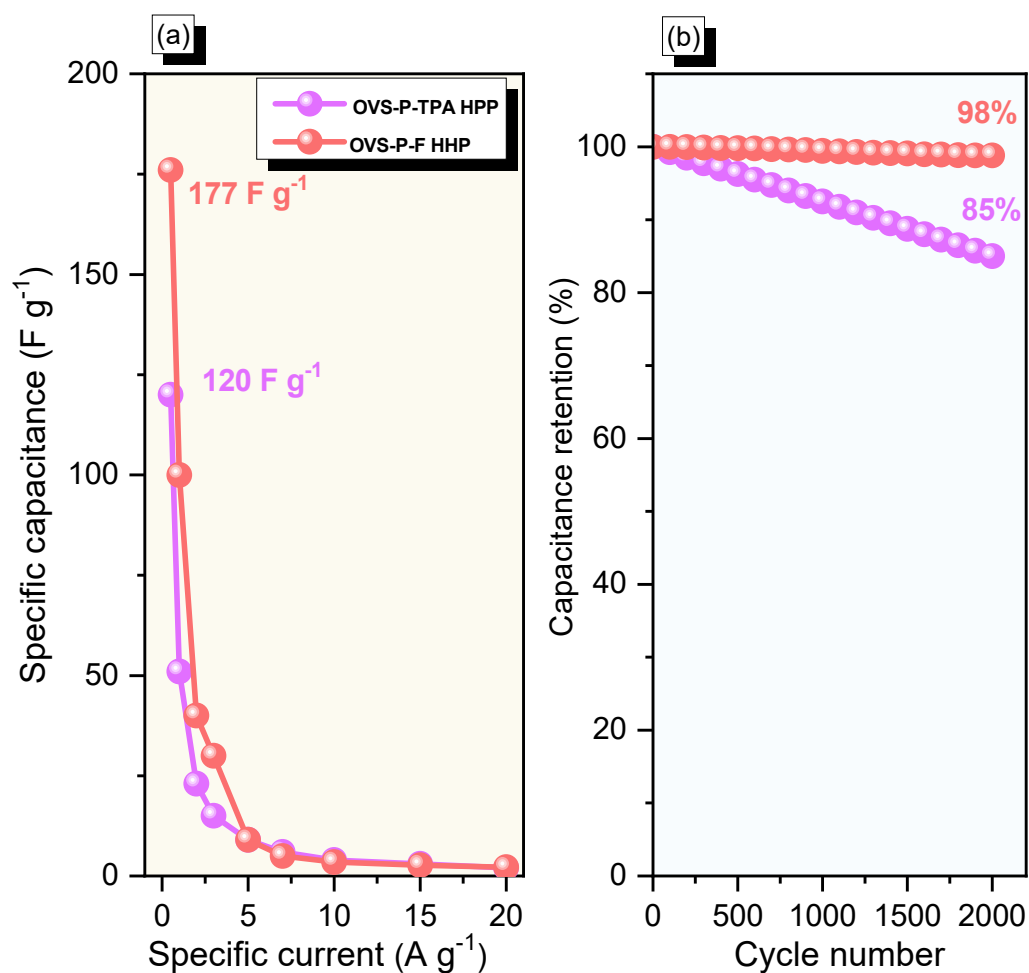


Figure 8. (a) Specific capacitance and (b) stability profiles for OVS-A HPP and OVS-P-A HPP.

In addition, we examined the electrochemical properties of the OVS-A HPP and OVS-P-A HPP for a symmetric supercapacitor using coin cells (Figure S4). The CV profiles of OVS-A HPP and OVS-P-A HPP were measured at the same scan rates and potential windows as the three electrodes (Figure S4a,b). The CV curve for OVS-A HPP (Figure S4a) is quite similar to the three-electrode system, but in OVS-P-A HPP (Figure S4b), the humps appeared more prominently to assist in the presence of both EDLC and pseudocapacitance. The pure triangular GCD curve was observed for OVS-A HPP, suggesting the presence of EDLC (Figure S4c), and OVS-P-A HPP experienced a triangular curve with

some bends demonstrating EDLC and a pseudocapacitive response (Figure S4d). The specific capacity was observed as 33 F g^{-1} and 80 F g^{-1} for OVS-A HPP and OVS-P-A at 0.5 A g^{-1} , respectively. Therefore, two and three electrodes revealed the significant electrochemical performance of OVS-A HPP and OVS-P-A HPP. Based on the two-electrode system, the OVS-P-A HPP had a better energy density (40 Wh Kg^{-1}) than the OVS-A HPP (16 Wh Kg^{-1}) (Figure S5).

3. Materials and Methods

3.1. Materials

We ordered potassium carbonate (K_2CO_3), nitrobenzene ($\text{C}_6\text{H}_5\text{NO}_2$), bromine solution (Br_2), and octavinylsilsesquioxane (OVS) from Alfa Aesar. Acros Organics provided acetone, methanol (MeOH), chloroform (CHCl_3), and tetrahydrofuran (THF), as well as N,N-dimethylformamide (DMF), and methanol (MeOH). Anthracene (A), pyrene (P), and tetrakis (triphenylphosphine) palladium (0) [$\text{Pd}(\text{PPh}_3)_4$] were supplied from Sigma-Aldrich. The instrumental methods and electrochemical experimental conditions can be found in the Supplementary File.

3.2. Synthesis of 9,10-Dibromoanthracene (A- Br_2)

Anthracene (5.00 g, 2.80 mmol), Br_2 (12.5 mL), and CHCl_3 were added to a two-neck flask and heated at $60 \text{ }^\circ\text{C}$ in an N_2 environment for 5 h. After that, the yellow solid (A- Br_2 , 85%) was filtered. $^1\text{H-NMR}$ (500 MHz, CDCl_3 , Figure S1): 8.6 (s, 2H), 7.6 (s, 2H). $^{13}\text{C-NMR}$ (124 MHz, CDCl_3 , Figure S2): 133, 128, 127, 123.

3.3. Synthesis of 1,3,6,8-Tetrabromopyrene (P- Br_4)

Pyrene (6.00 g, 30 mmol), Br_2 (12 mL), and $\text{C}_6\text{H}_5\text{NO}_2$ (200 mL) were added to a two-neck flask and heated at $120 \text{ }^\circ\text{C}$ in an N_2 environment for 24 h; after that, the yellow solid (P- Br_4 , 91%) was filtered and washed by EtOH and dried under reduced pressure before it was used in the reaction. The NMR data of P- Br_4 were not provided in this work due to its poor solubility in all organic solvents.

3.4. Synthesis of OVS-A HPP and OVS-P-A HPP

OVS (0.40 g, 0.63 mmol), A- Br_2 (0.85 g, 2.53 mmol), [P- Br_4 (0.003 g, 0.064 mmol)/A- Br_2 (0.81 g, 2.41 mmol)], K_2CO_3 (3 g) and $\text{Pd}(\text{PPh}_3)_4$ (0.08 g) in DMF (30 mL), were added to the two-neck flask, and the reaction mixture was refluxed for 72 h at $110 \text{ }^\circ\text{C}$. Then, the resulting solid was washed with different solvents (THF, methanol, and acetone) to obtain a green powder (0.38 g, 95%) for OVS-A HPP or a yellow powder (0.30 g, 75%) for OVS-P-A HPP. The instrumental methods and experimental conditions can be found in the Supplementary File.

4. Conclusions

Two different hybrid porous polymers of OVS-A HPP and OVS-P-A HPP were successfully synthesized through the Heck reaction of OVS with anthracene and pyrene/anthracene. N_2 isothermal profiles showed the presence of micro and mesoporous properties in them with BET surfaces of $433 \text{ m}^2 \text{ g}^{-1}$ and $98 \text{ m}^2 \text{ g}^{-1}$ for OVS-A HPP and OVS-P-A HPP, respectively. The TGA analysis revealed that OVS-A HPP experienced a higher thermal stability and char yield ($579 \text{ }^\circ\text{C}$ and 83 wt%) than OVS-P-A HPP ($377 \text{ }^\circ\text{C}$ and 73 wt%) due to the higher cross-linking density of anthracene with OVS. Furthermore, the specific capacitance of OVS-A HPP and OVS-P-A HPP was 120 F g^{-1} and 177 F g^{-1} , respectively. The electrochemical analysis demonstrated that OVS-P-A HPP exhibited higher super-capacitive performance than OVS-A HPP and the other reported porous polymer materials.

Supplementary Materials: The supporting information can be downloaded at: <https://www.mdpi.com/article/10.3390/ijms24032501/s1>.

Author Contributions: M.E., M.G.M. and M.M.S. conceptualized and designed the project; M.E. and M.G.M. performed the experiments; M.E., M.G.M., Y.Y. and M.M.S. analyzed the data; M.E. and M.G.M. wrote the original draft and edited the manuscript; M.G.M. and S.-W.K. supervision. All authors have read and agreed to the published version of the manuscript.

Funding: This study was supported financially by the Ministry of Science and Technology, Taiwan, under contracts NSTC 110-2124-M-002-013 and 111-2223-E-110-004.

Institutional Review Board Statement: Not applicable.

Informed Consent Statement: Not applicable.

Data Availability Statement: The data presented in this study are available on request from the corresponding author.

Acknowledgments: The authors thank the staff at National Sun Yat-sen University for their assistance with the TEM (ID: EM022600) experiments.

Conflicts of Interest: The authors declare no conflict of interest.

References

1. Liu, S.; Kang, L.; Zhang, J.; Jung, E.; Lee, S.; Jun, S.C. Structural engineering and surface modification of MOF-derived cobalt-based hybrid nanosheets for flexible solid-state supercapacitors. *Energy Storage Mater.* **2020**, *32*, 167–177. [[CrossRef](#)]
2. Mohamed, M.G.; Elsayed, M.E.; Ye, Y.; Samy, M.M.; Hassan, A.E.; Mansoure, T.H.; Wen, Z.; Chou, H.H.; Chen, K.H.; Kuo, S.W. Construction of Porous Organic/Inorganic Hybrid Polymers Based on Polyhedral Oligomeric Silsesquioxane for Energy Storage and Hydrogen Production from Water. *Polymers* **2023**, *15*, 182. [[CrossRef](#)]
3. Huang, Q.; Wang, J.; Gong, H.; Zhang, Q.; Wang, M.; Wang, W.; Nshimiyimana, J.P.; Diao, X. A rechargeable electrochromic energy storage device enabling effective energy recovery. *J. Mater. Chem. A* **2021**, *9*, 6451–6459. [[CrossRef](#)]
4. Weng, T.H.; Mohamed, M.G.; Sharma, S.U.; Chaganti, S.V.; Samy, M.M.; Lee, J.T.; Kuo, S.W. Ultrastable Three-Dimensional Triptycene- and Tetraphenylethene-Conjugated Microporous Polymers for Energy Storage. *ACS Appl. Energy Mater.* **2022**, *5*, 14239–14249. [[CrossRef](#)]
5. Weng, Z.; Su, Y.; Wang, D.W.; Li, F.; Du, J.; Cheng, H.M. Graphene–cellulose paper flexible supercapacitors. *Adv. Energy Mater.* **2011**, *1*, 917–922. [[CrossRef](#)]
6. Samy, M.M.; Mohamed, M.G.; Sharma, S.U.; Chaganti, S.V.; Mansoure, T.H.; Lee, J.T.; Chen, T.; Kuo, S.W. Constructing conjugated microporous polymers containing triphenylamine moieties for high-performance capacitive energy storage. *Polymer* **2023**, *264*, 125541. [[CrossRef](#)]
7. Samy, M.M.; Sharma, S.U.; Mohamed, M.G.; Mohammed, A.A.K.; Chaganti, S.V.; Lee, J.T.; Kuo, S.W. Conjugated microporous polymers containing ferrocene units for high carbon dioxide uptake and energy storage. *Mater. Chem. Phys.* **2022**, *287*, 126177. [[CrossRef](#)]
8. Xu, Z.; Sun, S.; Han, Y.; Wei, Z.; Cheng, Y.; Yin, S.; Cui, W. High-Energy-Density Asymmetric Supercapacitor Based on a Durable and Stable Manganese Molybdate Nanostructure Electrode for Energy Storage Systems. *ACS Appl. Energy Mater.* **2020**, *3*, 5393–5404. [[CrossRef](#)]
9. Mohamed, M.G.; Chaganti, S.V.; Sharma, S.U.; Samy, M.M.; Ejaz, M.; Lee, J.T.; Zhang, K.; Kuo, S.W. Constructing Conjugated Microporous Polymers Containing the Pyrene-4,5,9,10-Tetraone Unit for Energy Storage. *ACS Appl. Energy Mater.* **2022**, *5*, 10130–10140. [[CrossRef](#)]
10. Wang, Q.; Zhu, M.; Chen, G.; Dudko, N.; Li, Y.; Liu, H.; Shi, L.; Wu, G.; Zhang, D. High-Performance Microsized Si Anodes for Lithium-Ion Batteries: Insights into the Polymer Configuration Conversion Mechanism. *Adv. Mater.* **2022**, *34*, 2109658. [[CrossRef](#)]
11. Roh, D.H.; Shin, H.; Kim, H.T.; Kwon, T.H. Sono-Cavitation and Nebulization-Based Synthesis of Conjugated Microporous Polymers for Energy Storage Applications. *ACS Appl. Mater. Interfaces* **2021**, *13*, 61598–61609. [[CrossRef](#)] [[PubMed](#)]
12. Wang, Y.; Li, W.; Zhang, L.; Zhang, X.; Tan, B.; Hao, J.; Zhang, J.; Wang, X.; Hu, Q.; Lu, X. Amorphous Cobalt Hydrogen Phosphate Nanosheets with Remarkable Electrochemical Performances as Advanced Electrode for Supercapacitors. *J. Power Sources* **2020**, *449*, 227487. [[CrossRef](#)]
13. Kim, D.; Kang, J.; Yan, B.; Seong, K.; Piao, Y. Ambient Temperature Synthesis of Iron-Doped Porous Nickel Pyrophosphate Nanoparticles with Long-Term Chemical Stability for High-Performance Oxygen Evolution Reaction Catalysis and Supercapacitors. *ACS Sustain. Chem. Eng.* **2020**, *8*, 2843–2853. [[CrossRef](#)]
14. Wang, H.; Cheng, Z.; Liao, Y.; Li, J.; Weber, J.; Thomas, A.; Faul, C.F.J. Conjugated Microporous Polycarbazole Networks as Precursors for Nitrogen-Enriched Microporous Carbons for CO₂ Storage and Electrochemical Capacitors. *Chem. Mater.* **2017**, *29*, 4885–4893. [[CrossRef](#)]

15. Mei, L.; Wei, J.-C.; Duan, Q. Construction of copper porphyrinlinked conjugated microporous polymer/carbon nanotube composite as flexible electrodes for supercapacitors. *J. Mater. Sci. Mater. Electron.* **2021**, *32*, 24953–24963. [[CrossRef](#)]
16. Samy, M.M.; Mohamed, M.G.; Kuo, S.W. Pyrene-functionalized tetraphenylethylene polybenzoxazine for dispersing single-walled carbon nanotubes and energy storage. *Compos. Sci. Technol.* **2020**, *199*, 108360. [[CrossRef](#)]
17. Najib, S.; Erdem, E. Current progress achieved in novel materials for supercapacitor electrodes: Mini review. *Nanoscale Adv.* **2019**, *1*, 2817–2827. [[CrossRef](#)]
18. Zhao, C.; Jia, X.; Shu, K.; Yu, C.; Wallace, G.G.; Wang, C. Conducting polymer composites for unconventional solid-state supercapacitors. *J. Mater. Chem. A* **2020**, *8*, 4677–4699. [[CrossRef](#)]
19. Zhu, T.; Yang, Y.; Liu, Y.; Lopez-Hallman, R.; Ma, Z.; Liu, L.; Gong, X. Wireless portable light-weight self-charging power packs by perovskite-organic tandem solar cells integrated with solid-state asymmetric supercapacitors. *Nano Energy* **2020**, *78*, 105397. [[CrossRef](#)]
20. Mohamed, M.M.; EL-Mahdy, A.F.M.; Kotp, M.G.; Kuo, S.W. Advances in porous organic polymers: Syntheses, structures, and diverse applications. *Mater. Adv.* **2022**, *3*, 707–733. [[CrossRef](#)]
21. Zheng, S.; Miao, L.; Sun, T.; Li, L.; Ma, T.; Bao, J.; Tao, Z.; Chen, J. An extended carbonyl-rich conjugated polymer cathode for high-capacity lithium-ion batteries. *J. Mater. Chem. A* **2021**, *9*, 2700–2705. [[CrossRef](#)]
22. Mohamed, M.G.; Chaganti, S.V.; Li, M.S.; Samy, M.M.; Sharma, S.U.; Lee, J.T.; Elsayed, M.H.; Chou, H.H.; Kuo, S.W. Ultrastable Porous Organic Polymers Containing Thianthrene and Pyrene Units as Organic Electrode Materials for Supercapacitors. *ACS Appl. Energy Mater.* **2022**, *5*, 6442–6452. [[CrossRef](#)]
23. Mohamed, M.G.; Ahmed, M.M.M.; Du, W.T.; Kuo, S.W. Meso/Microporous Carbons from Conjugated Hyper-Crosslinked Polymers Based on Tetraphenylethylene for High-Performance CO₂ Capture and Supercapacitor. *Molecules* **2021**, *26*, 738. [[CrossRef](#)]
24. Mohamed, M.G.; Atayde, E.C., Jr.; Matsagar, M.B.; Na, J.; Yamauchi, Y.; Wu, K.C.W.; Kuo, S.W. Construction Hierarchically Mesoporous/Microporous Materials Based on Block Copolymer and Covalent Organic Framework. *J. Taiwan Inst. Chem. Eng.* **2020**, *112*, 180–192. [[CrossRef](#)]
25. Kim, J.; Kim, J.H.; Ariga, K. Redox-Active Polymers for Energy Storage Nanoarchitectonics. *Joule* **2017**, *1*, 739–768. [[CrossRef](#)]
26. Amin, K.; Ashraf, N.; Mao, L.; Faul, C.F.J.; Wei, Z. Conjugated microporous polymers for energy storage: Recent progress and challenges. *Nano Energy* **2021**, *85*, 105958. [[CrossRef](#)]
27. Mohamed, M.G.; Chang, W.C.; Kuo, S.W. Crown Ether- and Benzoxazine-Linked Porous Organic Polymers Displaying Enhanced Metal Ion and CO₂ Capture through Solid-State Chemical Transformation. *Macromolecules* **2022**, *55*, 7879–7892. [[CrossRef](#)]
28. Wang, H.; Li, Z.; Meng, Z.; Guo, X.; Du, Y.; Yang, H. An easily obtained hypercrosslinked pyrene-based porous organic polymer as a high performance electrode material for lithium-ion batteries. *New J. Chem.* **2021**, *45*, 7060–7064. [[CrossRef](#)]
29. Khattak, A.M.; Sin, H.; Ghazi, Z.A.; He, X.; Liang, B.; Khan, N.A.; Alanagh, H.R.; Iqbal, A.; Li, L.S.; Tang, Z.T. Controllable fabrication of redox-active conjugated microporous polymer on reduced graphene oxide for high performance faradaic energy storage. *J. Mater. Chem. A* **2018**, *6*, 18827–18832. [[CrossRef](#)]
30. Samy, M.M.; Mohamed, M.G.; Kuo, S.W. Directly synthesized nitrogen-and-oxygen-doped microporous carbons derived from a bio-derived polybenzoxazine exhibiting high-performance supercapacitance and CO₂ uptake. *Eur. Polym. J.* **2020**, *138*, 109954. [[CrossRef](#)]
31. Lyu, W.; Yan, C.; Chen, Z.; Chen, J.; Zuo, H.; Teng, L.; Liu, H.; Wang, L.; Liao, Y. Spirobifluorene-Based Conjugated Microporous Polymer-Grafted Carbon Nanotubes for Efficient Supercapacitive Energy Storage. *ACS Appl. Energy Mater.* **2022**, *5*, 3706–3714. [[CrossRef](#)]
32. Cai, G.; Cui, P.; Shi, W.; Morris, S.; Lou, S.N.; Chen, J.; Ciou, J.H.; Paidi, V.K.; Lee, K.S.; Li, S.; et al. One-Dimensional π -d Conjugated Coordination Polymer for Electrochromic Energy Storage Device with Exceptionally High Performance. *Adv. Sci.* **2020**, *7*, 1903109. [[CrossRef](#)] [[PubMed](#)]
33. Mohamed, M.G.; Chen, T.C.; Kuo, S.W. Solid-State Chemical Transformations to Enhance Gas Capture in Benzoxazine-Linked Conjugated Microporous Polymers. *Macromolecules* **2021**, *54*, 5866–5877. [[CrossRef](#)]
34. Borenstein, A.; Hanna, O.; Attias, R.; Luski, S.; Brousse, T.; Aurbach, D. Carbon-based composite materials for supercapacitor electrodes: A review. *J. Mater. Chem. A* **2017**, *5*, 12653–12672. [[CrossRef](#)]
35. Li, L.; Lu, F.; Xue, R.; Ma, B.L.; Li, Q.; Wu, N.; Liu, H.; Yao, W.Q.; Guo, H.; Yang, W. Ultrastable triazine-based covalent organic framework with an interlayer hydrogen bonding for supercapacitor applications. *ACS Appl. Mater. Interfaces* **2019**, *11*, 26355–26363. [[CrossRef](#)] [[PubMed](#)]
36. Mohamed, M.G.; Sharma, S.U.; Yang, C.H.; Samy, M.M.; Mohammed, A.A.K.; Chaganti, S.V.; Lee, J.T.; Kuo, S.W. Anthraquinone-Enriched Conjugated Microporous Polymers as Organic Cathode Materials for High-Performance Lithium-Ion Batteries. *ACS Appl. Energy Mater.* **2021**, *4*, 14628–14639. [[CrossRef](#)]
37. Mohamed, M.G.; Samy, M.M.; Mansoure, T.H.; Sharma, S.U.; Tsai, M.S.; Chen, J.H.; Lee, J.T.; Kuo, S.W. Dispersions of 1,3,4-Oxadiazole-Linked Conjugated Microporous Polymers with Carbon Nanotubes as a High-Performance Electrode for Supercapacitors. *ACS Appl. Energy Mater.* **2022**, *5*, 3677–3688. [[CrossRef](#)]
38. Mohamed, M.G.; Elsayed, M.H.; Elewa, A.M.; EL-Mahdy, A.F.M.; Yang, C.H.; Mohammed, A.A.K.; Chou, H.H.; Kuo, S.W. Pyrene-containing conjugated organic microporous polymers for photocatalytic hydrogen evolution from water. *Catal. Sci. Technol.* **2021**, *11*, 2229–2241. [[CrossRef](#)]

39. Das, S.; Heasman, P.; Ben, T.; Qiu, S. Porous organic materials: Strategic design and structure–function correlation. *Chem. Rev.* **2017**, *117*, 1515–1563. [[CrossRef](#)] [[PubMed](#)]
40. Samy, M.M.; Mekhemer, I.M.A.; Mohamed, M.G.; Elsayed, M.H.; Lin, K.H.; Chen, Y.K.; Wu, T.L.; Chou, H.H.; Kuo, S.W. Conjugated microporous polymers incorporating Thiazolo[5,4-d]thiazole moieties for Sunlight-Driven hydrogen production from water. *Chem. Eng. J.* **2022**, *446*, 137158. [[CrossRef](#)]
41. Wang, C.; Zhou, L.; Du, Q.; Shan, T.; Zheng, K.; He, J.; He, H.; Chen, S.; Wang, X. Synthesis, properties and applications of well-designed hybrid polymers based on polyhedral oligomeric silsesquioxane. *Polym. Int.* **2022**, *71*, 379–392. [[CrossRef](#)]
42. Ju, J.G.; Fejjaria, K.; Cheng, Y.; Liu, M.Y.; Lia, Z.J.; Kang, W.M.; Liao, Y. Engineering hierarchically structured superhydrophobic PTFE/POSS nanofibrous membranes for membrane distillation. *Desalination* **2020**, *486*, 114481. [[CrossRef](#)]
43. Mohamed, M.G.; Kuo, S.W. Functional Silica and Carbon Nanocomposites Based on Polybenzoxazines. *Macromol. Chem. Phys.* **2019**, *220*, 1800306. [[CrossRef](#)]
44. Strachota, B.; Matějka, L.; Hodan, J.; Kobera, L.; Mahun, A.; Dybal, J.; Šlouf, M. Polyhedral oligomeric silsesquioxane (POSS)-based epoxy nanocomposite involving a reversible Diels–Alder-type network as a self-healing material. *J. Adhes. Sci. Technol.* **2021**, *35*, 2736–2757. [[CrossRef](#)]
45. Feng, L.; Zhao, P.; Chen, T.; Jing, M. Study on the Influence of Nano-OvPOSS on the Compatibility, Molecular Structure, and Properties of SBS Modified Asphalt by Molecular Dynamics Simulation. *Polymers* **2022**, *14*, 4121. [[CrossRef](#)]
46. Sun, X.; Wang, J.; Fu, Q.; Zhang, Q.; Xu, R. Synthesis of a Novel Bifunctional Epoxy Double-Decker Silsesquioxane: Improvement of the Thermal Stability and Dielectric Properties of Polybenzoxazine. *Polymers* **2022**, *14*, 5154. [[CrossRef](#)]
47. Chen, Y.; Fang, Y.; Yu, J.; Gao, W.; Zhao, H.; Zhang, X. A silsesquioxane-porphyrin-based porous organic polymer as a highly efficient and recyclable absorbent for wastewater treatment. *J. Hazard. Mater.* **2021**, *406*, 124769. [[CrossRef](#)]
48. Wang, Q.; Unno, M.; Liu, H. Silsesquioxane-Based Triphenylamine-Linked Fluorescent Porous Polymer for Dyes Adsorption and Nitro-Aromatics Detection. *Materials* **2021**, *14*, 3851. [[CrossRef](#)]
49. Duszczak, J.; Mituła, K.; Portillo, A.S.; Soumoy, L.; Rzonowska, M.; Januszewski, R.; Fusaro, L.; Aprile, C.; Dudzic, B. Double-Decker Silsesquioxanes Self-Assembled in One-Dimensional Coordination Polymeric Nanofibers with Emission Properties. *ACS Appl. Mater. Interfaces* **2021**, *13*, 22806–22818. [[CrossRef](#)]
50. Tanaka, T.; Hasegawa, Y.; Kawamori, T.; Kunthom, R.; Takeda, N.; Unno, M. Synthesis of Double-Decker Silsesquioxanes from Substituted Difluorosilane. *Organometallics* **2019**, *38*, 743–747. [[CrossRef](#)]
51. Chen, F.; Lin, F.; Zhang, Q.; Cai, R.; Wu, Y.; Ma, X. Polyhedral Oligomeric Silsesquioxane Hybrid Polymers: Well-Defined Architectural Design and Potential Functional Applications. *Macromol. Rapid Commun.* **2019**, *40*, 1900101. [[CrossRef](#)]
52. Shi, H.; Yang, J.; You, M.; Li, Z.; He, C. Polyhedral Oligomeric Silsesquioxanes (POSS)-Based Hybrid Soft Gels: Molecular Design, Material Advantages, and Emerging Application. *ACS Mater. Lett.* **2020**, *2*, 296–316. [[CrossRef](#)]
53. Ejaz, M.; Mohamed, M.G.; Sharma, S.U.; Lee, J.T.; Huang, C.F.; Chen, T.; Kuo, S.W. An Ultrastable Porous Polyhedral Oligomeric Silsesquioxane/Tetraphenylthiophene Hybrid as a High-Performance Electrode for Supercapacitors. *Molecules* **2022**, *27*, 6238. [[CrossRef](#)]
54. Mohamed, M.G.; Kuo, S.W. Progress in the self-assembly of organic/inorganic polyhedral oligomeric silsesquioxane (POSS) hybrids. *Soft Matter* **2022**, *18*, 5535–5561. [[CrossRef](#)]
55. Mohamed, M.G.; Mansoure, T.H.; Takashi, Y.; Samy, M.M.; Chen, T.; Kuo, S.W. Ultrastable porous organic/inorganic polymers based on polyhedral oligomeric silsesquioxane (POSS) hybrids exhibiting high performance for thermal property and energy storage. *Microporous Mesoporous Mater.* **2021**, *328*, 111505. [[CrossRef](#)]
56. Du, Y.; Liu, H. Cage-like silsesquioxanes-based hybrid materials. *Dalton Trans.* **2020**, *49*, 5396–5405. [[CrossRef](#)]
57. Kuo, S.W. Hydrogen bonding interactions in polymer/polyhedral oligomeric silsesquioxane nanomaterials. *J. Polym. Res.* **2022**, *29*, 69. [[CrossRef](#)]
58. Joshi, M.; Butola, B.S. Polymeric nanocomposites-Polyhedral oligomeric silsesquioxanes (POSS) as hybrid nanofiller. *J. Macromol. Sci.-Polym. Rev.* **2004**, *44*, 389–410. [[CrossRef](#)]
59. Kong, D.; Cai, T.; Fan, H.; Hu, H.; Wang, X.; Cui, Y.; Wang, D.; Wang, Y.; Hu, H.; Wu, M.; et al. Polycyclic Aromatic Hydrocarbons as a New Class of Promising Cathode Materials for Aluminum-Ion Batteries. *Angew. Chem. Int. Ed.* **2022**, *61*, e202114681. [[CrossRef](#)]
60. Das, S.; Bhauriyal, P.; Pathak, B. Polycyclic Aromatic Hydrocarbons as Prospective Cathodes for Aluminum Organic Batteries. *J. Phys. Chem. C* **2021**, *125*, 49–57. [[CrossRef](#)]
61. Kagatkar, S.; Sunil, D.; Kekuda, D.; Satyanarayana, M.N.; Kulkarni, S.D.; Sudhakar, Y.N.; Vatti, A.K.; Sadhanala, A. Pyrene-based chalcones as functional materials for organic electronics application. *Mater. Chem. Phys.* **2022**, *293*, 126839. [[CrossRef](#)]
62. Mohamed, M.G.; Sharma, S.U.; Liu, N.Y.; Mansoure, T.H.; Samy, M.M.; Chaganti, S.V.; Chang, Y.L.; Lee, J.T.; Kuo, S.W. Ultrastable covalent triazine organic framework based on anthracene moiety as a platform for high-performance carbon dioxide adsorption and supercapacitors. *Int. J. Mol. Sci.* **2022**, *23*, 3174. [[CrossRef](#)]
63. Meng, Q.; Cai, K.; Chen, Y.; Chen, L. Research progress on conducting polymer based supercapacitor electrode materials. *Nano Energy* **2017**, *36*, 268–285. [[CrossRef](#)]
64. Gao, Y. Graphene and polymer composites for supercapacitor applications: A review. *Nanoscale Res. Lett.* **2017**, *12*, 387. [[CrossRef](#)]
65. Shrivastav, V.; Sundriyal, S.; Kim, K.H.; Sinha, R.K.; Tiwari, U.K.; Deep, A. Metal-organic frameworks-derived titanium dioxide-carbon nanocomposite for supercapacitor applications. *Int. J. Energy Res.* **2020**, *44*, 6269–6284. [[CrossRef](#)]

66. Tomboc, G.M.; Kim, H. Derivation of both EDLC and pseudocapacitance characteristics based on synergistic mixture of NiCo₂O₄ and hollow carbon nanofiber: An efficient electrode towards high energy density supercapacitor. *Electrochim. Acta* **2019**, *318*, 392–404. [[CrossRef](#)]
67. Velásquez, J.D.; Tomczykowa, M.; Plonska-Brzezinska, M.E.; Chaur, M.N. Evaluation of the covalent functionalization of carbon nano-onions with pyrene moieties for supercapacitor applications. *Materials* **2020**, *13*, 1141. [[CrossRef](#)]
68. Wang, Y.; Chen, F.; Liu, Z.; Tang, Z.; Yang, Q.; Zhao, Y.; Du, S.; Chen, Q.; Zhi, C. A highly elastic and reversibly stretchable all-polymer supercapacitor. *Angew. Chem.* **2019**, *131*, 15854–15858. [[CrossRef](#)]
69. Saber, A.F.; Sharma, S.U.; Lee, J.T.; EL-Mahdy, A.F.; Kuo, S.W. Carbazole-conjugated microporous polymers from Suzuki–Miyaura coupling for supercapacitors. *Polymer* **2022**, *254*, 125070. [[CrossRef](#)]
70. Xu, L.; Shi, R.; Li, H.; Han, C.; Wu, M.; Wong, C.P. Kang, F.; Li, B. Pseudocapacitive anthraquinone modified with reduced graphene oxide for flexible symmetric all-solid-state supercapacitors. *Carbon* **2018**, *127*, 459–468. [[CrossRef](#)]
71. Guo, B.; Yang, Y.; Hu, Z.; An, Y.; Zhang, Q.; Yang, X.; Wang, X.; Wu, H. Redox-active organic molecules functionalized nitrogen-doped porous carbon derived from metal-organic framework as electrode materials for supercapacitor. *Electrochim. Acta* **2017**, *223*, 74–84. [[CrossRef](#)]
72. Mohamed, M.G.; Zhang, X.; Mansoure, T.H.; El-Mahdy, A.F.M.; Huang, C.F.; Danko, M.; Xin, Z.; Kuo, S.W. Hypercrosslinked porous organic polymers based on tetraphenylanthraquinone for CO₂ uptake and high-performance supercapacitor. *Polymer* **2020**, *205*, 122857–122866. [[CrossRef](#)]
73. Mohamed, M.G.; El-Mahdy, A.F.M.; Meng, T.S.; Samy, M.M.; Kuo, S.W. Multifunctional Hypercrosslinked Porous Organic Polymers Based on Tetraphenylethene and Triphenylamine Derivatives for High-Performance Dye Adsorption and Supercapacitor. *Polymers* **2020**, *12*, 2426. [[CrossRef](#)] [[PubMed](#)]
74. Li, X.C.; Zhang, Y.; Wang, C.Y.; Wan, Y.; Lai, W.Y.; Pang, H.; Huang, W. Redox-active triazatruxene-based conjugated microporous polymers for high-performance supercapacitors. *Chem. Sci.* **2017**, *8*, 2959–2965. [[CrossRef](#)] [[PubMed](#)]
75. Mohamed, M.G.; Chen, W.C.; Mahdy, A.F.M.; Kuo, S.W. Porous organic/inorganic polymers based on double-decker silsesquioxane for high-performance energy storage. *J. Polym. Res.* **2021**, *28*, 219. [[CrossRef](#)]

Disclaimer/Publisher’s Note: The statements, opinions and data contained in all publications are solely those of the individual author(s) and contributor(s) and not of MDPI and/or the editor(s). MDPI and/or the editor(s) disclaim responsibility for any injury to people or property resulting from any ideas, methods, instructions or products referred to in the content.